Tellus SERIES B CHEMICAL AND PHYSICAL METEOROLOGY
PUBLISHED BY THE INTERNATIONAL METEOROLOGICAL INSTITUTE IN STOCKHOLM

Revised eddy covariance flux calculation methodologies – effect on urban energy balance

By ANNIKA NORDBO*, LEENA JÄRVI and TIMO VESALA, *Department of Physics, Division of Atmospheric Sciences and Geophysics, University of Helsinki, P.O. Box 48, 00014 Helsinki, Finland*

(Manuscript received 19 July 2011; in final form 27 January 2012)

ABSTRACT

Eddy covariance (EC) measurements of turbulent fluxes of momentum, sensible heat and latent heat – in addition to net radiation measurements – were conducted for three consecutive years in an urban environment: Helsinki, Finland. The aims were to: (1) quantify the detection limit and random uncertainty of turbulent fluxes, (2) assess the systematic error caused by EC calculation-procedure choices on the energy balance residual and (3) report the energy balance of the world's northernmost urban flux station. The mean detection limits were about 10% of the observed flux, and the random uncertainty was 9–16%. Of all fluxes, the latent heat flux – as measured with a closed-path gas analyser – was most prone to systematic calculation errors due to water vapour interactions with tube walls: using a lag window that is too small can cause a 15% lack of data (due to the dependency of lag time on relative humidity) and omitting spectral corrections can cause on average a 26% underestimation of the flux. The systematic errors in EC calculation propagate into the energy balance residual and can be larger than the residual itself: for example, omitting spectral corrections overestimates the residual by 13% or 18% on average, depending on the analyser.

Keywords: eddy covariance, urban, energy balance, flux uncertainty, flux error

1. Introduction

Approximately 75% of Europe's population lives in urban environments and a quarter of EU's land surface has been directly affected by urbanisation (EEA, 2006). This type of land-use change affects urban climate through alteration in surface–atmosphere interactions through energy fluxes. The urban surface energy balance of a building-air volume can be expressed as in the studies by Oke (1988), Offerle et al. (2005) and Sailor (2011)

$$R_n + Q_F - \Delta Q_S = H + LE + Q_A + \varepsilon_{EB}, \qquad (1)$$

where the left-hand side is the available energy with net radiation (R_n), anthropogenic heat release (Q_F, including buildings, transportation and human metabolism) and change in heat storage (ΔQ_S, including air, trees, buildings, soil, etc.). The right-hand side includes turbulent fluxes of sensible heat (H) and latent heat (LE) in addition to advection through the volume (Q_A), which is not readily measurable. The error term (ε_{EB}) that includes all other small processes such as precipitation is also assumed negligible. Direct measurement techniques of R_n are readily available, H and LE are measured using the only direct flux measurement technique, the eddy covariance (EC) method, but no standardised, direct methods for the estimation of Q_F and ΔQ_S are available. Consequently, these two terms are commonly treated together as the energy balance residual

$$Res = R_n - H - LE = \Delta Q_S - Q_F, \qquad (2)$$

which is negative when there is an additional energy source fueling H and LE, i.e. the building-air volume loses heat ($\Delta Q_S < 0$), there is an anthropogenic heat release ($Q_F > 0$), or both. The determination of Res suffers from the differences in energy flux source areas, which is a common and unavoidable problem in urban micrometeorological measurements (Oke, 2006).

As a consequence of the land cover changes that have led to the alteration of energy balance components, many models have been developed to describe this surface–atmosphere coupling (Grimmond et al., 2010, 2011). The increase in computation power has started to allow the inclusion of these processes to numerical weather prediction, and some operational weather prediction models already have urban environments incorporated in them

*Corresponding author.
email: annika.nordbo@helsinki.fi

Citation: Tellus B 2012, **64**, 18184, http://dx.doi.org/10.3402/tellusb.v64i0.18184

(Best, 2005). Nevertheless, there is still a shortage of observational studies of surface–atmosphere interactions in cities due to the diversity in city types and locations on Earth. Only within the past decade have EC flux measurements been conducted in urban environments. Most of the studies are concentrated on mid-latitude cities (Nemitz et al., 2002; Christen and Vogt, 2004; Grimmond et al., 2004; Rotach et al., 2005; Moriwaki and Kanda, 2006; Offerle et al., 2006; Pigeon et al., 2007; Lemonsu et al., 2008; Bergeron and Strachan, 2010; Wood et al., 2010) but recently also lower latitudes (<30°N, Frey et al., 2011) and higher latitudes (>60°N, Vesala et al., 2008) have been investigated.

Owing to the earlier start of turbulent flux measurements at non-urban sites, more effort on the methodological developments of the EC technique is made using data from, for example, forests, whereas such work with urban flux data is scarce. The turbulent fluxes over an urban surface differ from those over a forest due to a higher roughness, fraction of impervious surfaces and anthropogenic heat sources; and thus the atmosphere is less unstably stratified. The effect of EC calculation procedures on flux values at non-urban sites was extensively studied in Mauder and Foken (2006), Mauder et al. (2007) and Mauder et al. (2008), whereas Richardson et al. (2006), He et al. (2010) and Billesbach (2011) made an analysis on uncertainties incorporated in EC measurements at vegetative sites. Careful assessment of EC calculation procedures is needed in order to minimise systematic errors in flux calculations, and uncertainty analysis is important for assessing the systematic and unsystematic uncertainties incorporated in flux measurements. Uncertainty assessment is also vital for data assimilation (Raupach et al., 2005).

The quantification of errors stemming from EC calculation procedures and general EC flux uncertainty are especially important in urban environments, as the energy balance residual can be significant and cannot be easily measured (Grimmond and Oke, 1999; Christen and Vogt, 2004; Lemonsu et al., 2004; Bergeron and Strachan, 2010). Consequently, all errors made in the calculation of turbulent heat fluxes from EC data are propagated to the estimation of the anthropogenic heat release and heat storage change. For comparison, the energy balance at natural sites (without Q_F) is not usually closed and the EC method is suspected to underestimate the energy fluxes. The underestimation is commonly observed to be about 20% (Wilson et al., 2002; Launiainen, 2010; Nordbo et al., 2011). Thus, the residual of the energy balance gives an upper limit for the possible ΔQ_S and Q_F.

The aims of this study are (1) to quantify the random uncertainty and detection limit of turbulent urban heat fluxes, (2) to provide estimates for the systematic errors caused by combinations of EC flux calculations, (3) to assess the propagation of the systematic error into the urban energy balance residual term and (4) report 3 years' energy flux data for the world's northernmost urban EC flux measurement site.

2. Materials and methods

2.1. Study site

The measurements were conducted at the SMEAR III station (Station for Measuring Ecosystem-Atmosphere Relationships), 4 km north-east of downtown Helsinki, Finland. The station consists of (1) a 31-m-high lattice tower (60°12.17′N, 24°57.671′E in WGS84) and (2) rooftop measurements on top of a university building, which is 100 m north-east from the tower. The tower is located on a small hill, peaking at 29 m.a.s.l., with a deepest fall of 12° towards the south-east (120–180°, Fig. 1). The surroundings are characterised by heterogeneity, with surface coverage including impervious surfaces (such as buildings and parking lots), patchy forests and grassland. The area can be divided into three surface coverage sectors (urban 320–40°, road 40–180° and vegetation 180–320°) designated according to the dominant surface cover. The shortest distance to the shore line is 1 km, and no water surfaces are within the estimated flux footprint

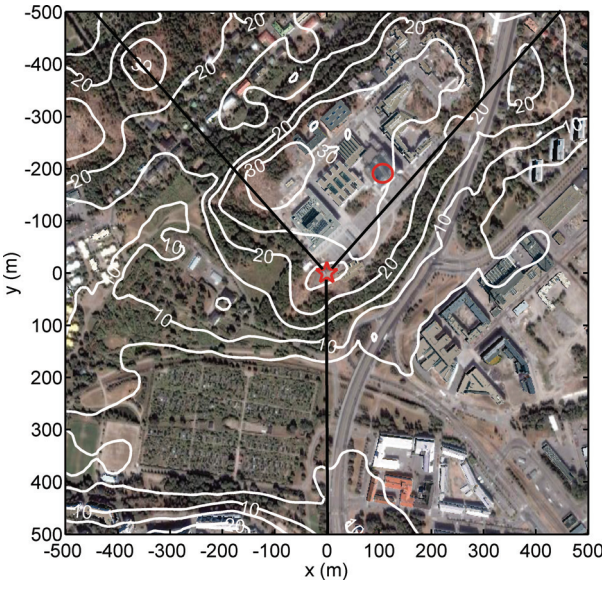

Fig. 1. An overview of the surrounding area of the EC tower: white height contour lines (m) superimposed on a Google Earth picture. The locations of the SMEAR III tower and the auxiliary meteorological instruments are marked with a red star and circle, respectively. Black lines indicate the borders of the three sectors (urban 320–40°, road 40–180° and vegetation 180–320°).

area (Vesala et al., 2008). Furthermore, the station has formed a part of the Helsinki Testbed project since its beginning (Koskinen et al., 2011). For further information on the station and the measurement site, see Vesala et al. (2008) and Järvi et al. (2009a,b).

The Helsinki metropolitan area (765 km^2) is the world's northernmost urban area among those with a population of over a million. The city is located on the coast of the Gulf of Finland and is the northernmost EU state capital. The weather is either marine or continental depending on the origin of the prevailing air mass, and the temperatures during winter are much higher than expected on the grounds of the latitude due to the mitigating effect of the North Atlantic Drift. However, the northern location causes a wide range in day length: sun-lit hours are 6 and 19 hours at the winter and summer solstices, respectively. The climatological monthly mean temperatures (1971–2000) range from $-4.9\,^{\circ}C$ for February to $17.2\,^{\circ}C$ for July, and the annual precipitation is 642 mm (Drebs et al., 2002).

2.2. Eddy covariance measurements

The eddy covariance method was used to measure turbulent fluxes of sensible and latent heat in addition to momentum. The measurements were made from the tower at 31 m height, and the setup consisted of a three-dimensional sonic anemometer (USA-1, Metek GmbH, Germany) for acquiring the three wind components and sonic temperature, and two infrared gas analysers for measuring the fluctuations in CO_2 and H_2O density and mixing ratio, respectively (open-path analyser LI-7500 and closed-path analyser LI-7000; LI-COR, Lincoln, NE, USA). The open-path analyser was set 20 cm below the anemometer, in a 30° slanted position to attempt to hinder rain droplets from staying in the measurement volume. Furthermore, a thermometer (semiconductor thermometer, LM335; National Semiconductor, Santa Clara, CA, USA) was placed on the LI-7500 in February 2009 to measure the analyser surface temperature. The closed-path analyser inlet was positioned 13 cm below the anemometer centre and air was drawn down to the infrared analyser through a 41 m length of steel tube, with an inner diameter of 8 mm and a mean flow rate of 17 l min^{-1}. The tube was heated (initially 4 W m^{-1}, and from 8 September 2010 onwards 16 W m^{-1}) to avoid water vapour condensation on tube walls. In addition, a mesh was installed to the inlet (acid-proof steel, diameter 6 mm, thickness 1 mm) and a filter was installed just before the analyser (PTFE filter, 1 μm pore size, diameter 50 mm, Gelman Acro 50) to prevent dirt from disturbing the measurements. Furthermore, the raw EC data were sampled at 10 Hz and stored for post-processing. The data were acquired between October 2007 and September 2010, representing three consecutive years.

2.3. Auxiliary meteorological measurements

In addition to the EC measurements, several meteorological variables were measured from the tower and the rooftop. Incoming and outgoing short- and long-wave radiation (CNR1; Kipp&Zonen, Delft, Netherlands) were measured from the tower at 31 m height to provide the net radiation, R_n. According to a cosine response, the 99% source area is a circle with a 31 m radius. The area consists of vegetation (45%), rock (35%) and impervious surface (20%); and the snow-free albedo is 0.15 ± 0.05 (mean and standard deviation, for times when global radiation input > 10 W m^{-2}). Data were divided into daytime and night-time observations using an incoming solar radiation limit of 4 W m^{-2}. Furthermore, air temperature (platinum resistant thermometer, Pt-100), air pressure (silicon aneroid barometer, Vaisala DPA500; Vaisala Oyj, Vantaa, Finland), relative humidity (RH, platinum resistance thermometer and thin film polymer sensor, Vaisala HMP243), wind speed (U, cup anemometer, Vaisala WAA141), wind direction (wind vane, Vaisala WAV151) and precipitation (rain gauge, Pluvio2, Ott Messtechnik GmbH, Germany) were measured at the rooftop site (24 m a.g.l., 51 m a.s.l.). Data were divided into thermal seasons according to the 5-d running mean temperature: spring and fall are periods with temperatures between 0 °C and 10 °C, and winter and summer have temperatures below 0 °C and over 10 °C, respectively. Snow cover is interpreted to prevail when the 5-d running-mean shortwave radiation albedo exceeds 0.3. This value is twice the albedo of the source area under the R_n measurements and is low enough to include both old and wet snow.

2.4. Eddy covariance calculations

The turbulent fluxes of sensible heat (H, W m^{-2}), latent heat (LE, W m^{-2}) and momentum (τ, kg m^{-2} s^{-2}) were measured with the above-described setup. The fluxes are calculated from covariances between a respective scalar and the vertical wind speed (w) as

$$H = \rho_a c_{pa} \overline{T'w'} \tag{3}$$

$$LE_{\mathrm{OP}} = L\overline{q'_{\mathrm{OP}}w'} \tag{4}$$

$$LE_{\mathrm{CP}} = L\rho_a \frac{M_w}{M_a} \overline{q'_{\mathrm{CP}}w'} \tag{5}$$

$$\tau = -\rho_a \sqrt{\overline{u'w'}^2 + \overline{v'w'}^2} = -\rho_a u_*^2, \tag{6}$$

where ρ_a (kg m^{-3}) is the density of air, $c_{pa} = 1004$ J kg^{-1} K^{-1} the specific heat of air at constant pressure and L (J kg^{-1}) the latent heat of vaporisation of

water, which was calculated as a function of air temperature according to Aubinet et al. (2000). T', w', u', v', q'_{OP} and q'_{CP} represent the deviations from the time averages of virtual temperature (K) (see Liu et al. 2001), vertical wind speed ($m\,s^{-1}$), two horizontal wind speed components ($m\,s^{-1}$), the water vapour density ($kg\,m^{-3}$) from the open-path analyser and water vapour mixing ratio ($mmol\,mol^{-1}$) from the closed-path analyser, respectively. M_w and M_a are the molar masses of water and air and u_* is the friction velocity ($m\,s^{-1}$). In this paper, the residual (eq. 2) calculated using LE_{OP} will be denoted Res_{OP} and likewise the residual using LE_{CP} is Res_{CP}. All turbulent heat fluxes are defined positive when directed upward.

Furthermore, the turbulent fluxes provide a possibility to calculate the dimensionless atmospheric stability $\zeta = \frac{z-d}{L}$, where z is the measurement height, d the displacement height and $L = -\frac{\rho_a c_{pa} u_*^3}{k\frac{g}{T}H}$ the Obukhov length (m, $k = 0.4$ and $g = 9.81\,m\,s^{-2}$). The sign of ζ is solely determined by the sign of H, and three stability categories are used in this paper: unstable ($\zeta < -0.01$), neutral ($-0.01 < \zeta < 0.01$) and stable ($\zeta > 0.01$).

However, the flux calculations are not as clear-cut as implied above: several steps have to be performed to gain more accurate flux estimates. In the following, 10 flux calculation procedures are represented. One calculation method combination is named standard, whereas others are obtained by making one modification to the standard calculation method combination at a time.

2.4.1. Standard calculation method combination. In the standard flux calculation method combination, the flux calculations start with raw data despiking and linear detrending (Table 1). Second, the 2-D rotation method is used to set the x-axis parallel to the mean wind direction and the vertical wind to zero. Third, the closed-path water vapour mixing ratio is converted relative to dry air to avoid dilution effects (Aubinet et al., 2000), and the density correction (Webb et al., 1980) becomes unnecessary as also the temperature fluctuations are dampened in the tube (Rannik et al., 1997). Fourth, the q'_{OP} and q'_{CP} time series are matched with the w' time series using the maximum cross-covariance method: the cross-correlation function is calculated by moving the two time series against each other within a lag window, and hereafter the maximum is located and its location gives the lag time (t_{lag}). The q'_{OP} time series were allowed to lag or lead w' by 1 s, whereas q'_{CP} could only lag w' as air needs time to pass through the 41 m sampling tube. Note that the lag window for q'_{CP} is much larger (up to 30 s) than for CO_2 because a strong RH dependency of the q'_{CP} lag time was observed (see Section 3.5). If a maximum cross-correlation could not be found, a mean value was used

Table 1. Calculation procedure comparison. The steps in eddy covariance raw data post-processing are shown in the columns, and the affected fluxes are in brackets: sensible heat (H) and open- and closed-path latent heat, (LE_{OP}, LE_{CP}). The names of the different calculation method combinations and their ID numbers are referred to in the text as rows. The calculation steps that are within the iteration are marked with a grey background. See text for further details

ID number		Averaging period (min)	Despiking and linear detrending	Coordinate rotation (all)	Relative to dry air (LE_{CP})	Lag time determination (all)	Cross-wind correction (H)	Iteration of fluxes (all)	Spectral correction (all)[a]	Sonic heat correction (H)	Density correction (LE_{OP})	Surface heating correction (LE_{OP})
1	Standard	30	x	2-D	x	x	x	x	exp	x	x	–
2	No spec.	30	x	2-D	x	x	x	x	–	x	x	–
3	Theor. spec.	30	x	2-D	x	x	x	x	theor	x	x	–
4	No iteration	30	x	2-D	x	x	x	–	exp	x	x	–
5	PF[b]	30	x	PF	x	x	x	x	exp	x	x	–
6	SHC	30	x	2-D	x	x	x	x	exp	x	x	x
7	Theor. lag[c]	30	x	2-D	x	theor	x	x	exp	x	x	–
8	5 min	5	x	2-D	x	x	x	x	exp	x	x	–
9	10 min	10	x	2-D	x	x	x	x	exp	x	x	–
10	20 min	20	x	2-D	x	x	x	x	exp	x	x	–
11	60 min	60	x	2-D	x	x	x	x	exp	x	x	–

[a]Experimental (exp) or theoretical (theor) spectral correction for LE_{CP}.
[b]PF = planar fitting somewhat as in Wilczak et al. (2001).
[c]Theoretical lag window for LE_{CP} as shown in Fig. 7.

for q'_{OP} and a *RH*-dependent value for q'_{CP}. The equations for t_{lag}(RH) are determined on a monthly basis following the maintenance (e.g. tube cleaning, filter changes) of the measurement system. Fifth, the raw covariances are obtained from the cross-covariance peak, and a cross-wind correction, as mentioned in the study by Liu et al. (2001), is applied to $\overline{w'T'}$.

Sixth, an iteration loop, which contains three corrections, starts. The iteration is needed because corrections are interrelated. Within the loop, spectral corrections to all covariances are made to account for low- and high-pass filtering. The underestimation of the low-frequency transport is caused by linear detrending (Rannik and Vesala, 1999) and a limited averaging period (Finnigan et al., 2003). Furthermore, the underestimation of the high-frequency transport is caused by the limited dynamic frequency response of the anemometer and gas analyser, the response mismatch between sensors, sensor separation, path averaging of the sonic and by path averaging of the open-path sensor or the attenuation of q'_{CP} in the sampling tube leading to the closed-path sensor (see e.g. Moncrieff et al., 1997).

Here, we perform the spectral corrections using the transfer function method initiated by Moore (1986) and further developed by Horst (1997, 2000) and Massman (2000, 2001). In the method, the flux attenuation (F_a, values between 0 and 1) is used for calculating the correct covariance $\left(\overline{w's'}_{corr}\right)$ from the measured one $\left(\overline{w's'}_{meas}\right)$ as

$$\overline{w's'}_{corr} = \frac{\overline{w's'}_{meas}}{F_a} \tag{7}$$

F_a is obtained by integrating a model co-spectrum ($C_{ws}(f)$) multiplied by a low and high frequency loss transfer function (TF_{LF}, TF_{HF}) as

$$F_a = \frac{\int_0^\infty TF_{LF}TF_{HF}(f)C_{ws}(f)df}{\int_0^\infty C_{ws}(f)df}, \tag{8}$$

where C_{ws} is the frequency-weighted cospectrum that is normalised by covariance and multiplied by natural frequency, f (Hz), see Appendix S1 in Supporting Information for the forms of co-spectra. Furthermore, the shape of TF_{HF} can be described solely by one variable, the response time (see e.g. Järvi et al., 2009a), which is then used for correcting the high-frequency loss.

The low-frequency transfer function is always determined theoretically (Rannik and Vesala, 1999), whereas the high-frequency transfer function (and thus the response time) can be estimated in several ways. We correct $\overline{w'T'}$, $\overline{w'q'_{OP}}$ and $\overline{u'w'}$ using the theoretical TF_{HF} formulae (Moncrieff et al., 1997) and $\overline{w'q'_{CP}}$ using experimental TF_{HF}. The closed-path water vapour measurements are treated differently because the q'_{CP} signal is known to be attenuated in the tube, and the attenuation is known to increase with *RH* (Ibrom et al., 2007; Massman and Ibrom, 2008) and tube age (Leuning and Judd, 1996; Su et al., 2004; Mammarella et al., 2009).

The transfer functions are calculated for about 1-month-long data sets that are further divided into seven different *RH* classes. For each period, TF_{HF} is gained by dividing the mean water vapour co-spectrum, with the mean temperature co-spectrum in a similar manner as in Mammarella et al. (2009) and Nordbo et al. (2011). The closed-path water vapour response time (t_{H_2O}) for a certain period can then be retrieved from a fit to TF_{HF}. The longer the response time, the larger the high-frequency loss.

After applying the spectral corrections within the iteration loop, sonic heating correction (Liu et al., 2001) is applied to $\overline{w'T'}$ using primarily $\overline{w'q'_{CP}}$, and a density correction (Webb et al., 1980) is applied to $\overline{w'q'_{OP}}$. The iteration is continued until the covariances change by less than 1%. The iteration is important because the changes in covariances affect the stability which in turn affects the spectral corrections.

2.4.2. Different calculation method combination. The above-described standard flux calculation method combination is altered in different ways to provide insight into the effect of calculation steps on the final flux estimates. Table 1 lists the different flux calculation methods, and different method combinations are given identification numbers (IDs) that are referred to in the following text.

The need of spectral corrections is assessed by leaving the corrections out (**ID2**) and by using the theoretical transfer functions (Moncrieff et al., 1997) instead of *RH*-dependent functions for $\overline{q'_{CP}w'}$ (**ID3**). Moreover, the effect of iteration is studied by discarding the interdependency of corrections (**ID4**). The coordinate rotation is also performed using an alternative technique: the planar fit method (Wilczak et al., 2001, **ID5**). In our version of the method, two tilt angles are derived from a three-dimensional planar fit to the three 30 min averaged wind components of individual 2-month periods. Within the periods, the data were divided into 18 wind direction planes to take into account the surrounding topography, which is so complex that it cannot be described even with higher-order planar fits (e.g. quadratic, not shown). The tilt angles are then used for rotating the winds of an individual 30 min period to streamline coordinates. This results in residual mean vertical wind velocities that are considered to be random noise or originate from large-scale motion. The mean of the standard deviations for all wind direction bins was 1.5 degrees for both tilt angles.

In addition to the above-mentioned modifications, still two adjustments are made to improve either the open- or

the closed-path evapotranspiration (E). A surface heating correction (Grelle and Burba, 2007; Burba et al., 2008; Järvi et al., 2009a) is performed to the open-path evapotranspiration to take into account the density fluctuations caused by the analyser itself (**ID6**). The corrected evapotranspiration is

$$E = E_0 + \delta \frac{(T_s - T_a)q}{r_r T_a}\left(1 + \mu \frac{\rho_v}{\rho_d}\right) \quad (9)$$

where E_0 is the WPL-corrected evaporation (mmol m^{-2} s^{-1}), δ the fraction of heat that stays in the boundary layer of the analyser and is relevant for the heating correction, T_s and T_a the surface and air temperatures (K), q the molar density of water vapour from the closed-path analyser (mol m^{-3}), r_r the aerodynamic transfer resistance (s m^{-1}, Uu_*^{-2}), μ the ratio between molar masses of air and water (1.6077) and ρ_v and ρ_d are the densities of water vapour and dry air, respectively (kg m^{-3}). The surface temperature can further be expressed as a function of air temperature $T_s = a_1 T_a + a_0$. Here, the fitting method introduced by Järvi et al. (2009a) was further developed. Data were divided into six radiation classes due to the strong relationship of the heating correction on solar radiation. For each radiation class, coefficients a_1 and a_0 were solved from the linear fitting between T_a and T_s measured at the open-path surface from February 2009 to September 2010. The measured T_s was also used in eq. (9) when δ was solved using the E from closed-path measurements and E_0 from WPL-corrected open-path measurements (see coefficients in Appendix S1 in Supporting Information). The coefficients were then used to correct the open-path E through the whole 3-yr measurement period.

The closed-path E, on the other hand, is largely effected by the processes in the sampling tube and filter, and thus a larger-than-normal lag window (6–30 s) was used for q'_{CP}. Consequently, it is worth making a comparison with LE_{CP} values gained using a 'theoretical lag window' and using mean lag values when a lag time is not found (**ID7**). Monthly checks were performed to the flow rate in the tube, leading to the closed-path analyser. The theoretical lag window was made to range from the theoretical lag time to twice its value as commonly done with closed-path measurements. For instance, for an average flow rate of 17 lpm, tube length 41 m, inner diameter 8 mm, the theoretical lag time would be $t_{lag} = 7.1$ s and the window would be 7.1–14.2 s. Linear dependency on time between measurement points was assumed.

Finally, as the last test, the averaging period was varied to be 5, 10, 30 and 60 min. The appropriate averaging time was also studied using Ogive analysis (Moncrieff et al., 2004). The Ogives were calculated for 219 min (2^{17} data points) periods starting every hour. These Ogives were then divided to three categories following Foken et al. (2006): (1) convergent Ogives within the 30 min interval, (2) Ogives with a distinct extreme value before the final value and (3) Ogives not convergent even for 219 min.

2.5. Flux quality assurance and uncertainty analysis methods

The EC data quality was assured using four methods. According to the stationarity test introduced by Foken and Wichura (1996), the flux covariance calculated for a 30 min interval should not deviate more than 30% from the mean of the covariances of 5 min subperiods. Furthermore, according to the intermittency test by Mahrt et al. (1998), the ratio of the standard deviation of the 5 min averaged flux to the absolute value of the 30 min averaged flux should not rise above unity. Finally, the skewness and kurtosis were to stay within the range of [−2, 2] and [1, 8] to ensure a near gaussian turbulent signal (Vickers and Mahrt, 1997). The latter two are applied to individual wind component and scalar time series, and they filter out spiked raw data efficiently. The stationarity and intermittency criteria filtered out H data, especially during sunrise and sunset, and LE data during night. The percentages of rejected data for all the fluxes are shown in Tables 1 and 2. In addition, 12.3% of flux data were omitted due to probable flow distortion when the wind was between 0° and 50°.

Table 2. Flux omittance percentages for momentum (τ), sensible heat (H) and closed- and open-path latent heat (LE_{CP}, LE_{OP}). Values are given for omittance due to all criteria for all data and for day- and night-time data, and for omittance only due to flux stationarity and intermittency. Also, the percentage of unacceptable skewness and kurtosis of the zonal wind (u), meridional wind (v), vertical wind (w), temperature (T), H_2O concentration from the open-path analyser (q_{OP}) and closed-path analyser (q_{CP}) are given. Values are calculated for raw 10 Hz data after despiking. See text for further details.

%	τ	H	LE_{OP}	LE_{CP}
All criteria	21.74	38.11	46.20	46.30
All criteria, day-time	19.64	40.05	48.69	57.05
All criteria, night-time	24.07	33.29	38.78	33.79
Flux stationarity	18.30	30.98	28.15	33.08
Flux intermittency	10.53	21.49	32.43	30.07

	u	v	w	T	q_{OP}	q_{CP}
Skewness	0.17	0.30	0.03	0.88	9.91	2.49
Kurtosis	0.55	0.97	0.25	2.42	12.8	7.69

In addition to the data quality assurance, the detection limit and random uncertainty for all fluxes were calculated. The detection limit, which quantifies the background noise, was defined somewhat following Wienhold et al. (1994). It was calculated as the standard deviation of the cross-covariance function at points ± 50 to 150 seconds around the maximum. In other words, a 3001-data-point-long cross-covariance vector with the real covariance at point 1501 is calculated, and the detection limit is further calculated as the standard deviation of the covariance at points 1–1000 and 2001–3001. Thus, the detection limit has units of covariance and can be converted to have units of flux. The random flux error, on the other hand, was calculated according to Lenschow et al. (1994) as

$$\sigma_F^2(\Gamma) \approx 2\frac{\Gamma_f}{\Gamma}\mu_F, \tag{10}$$

where Γ is the averaging period (30 min), Γ_f the integral time scale defined as the time point when the autocorrelation function of the covariance drops to $e^{-1} \approx 0.3679$ of its peak value and μ_F is the flux variance

$$\mu_F = \mu_s\mu_w + \overline{w's'}^2, \tag{11}$$

where μ_s and μ_w are the variances of the scalar s and w. The term $2\frac{\Gamma_f}{\Gamma}$ represents the error due to a finite flux averaging time that excludes the effect of larger eddies. In other words, shorter Γ_f gives faster covariance autocorrelation losses and a lesser effect of large eddies. Furthermore, μ_F describes the errors in the variance of the covariance. $\sigma_F^2(\Gamma)$ has units of covariance squared and can be converted to have units of flux. Random uncertainties at more homogeneous sites are often also calculated using the repeated sampling method (Hollinger and Richardson, 2005), but this procedure does not work for complex urban sites due to flux footprint issues and is thus not used in this study.

3. Results and discussion

3.1. Climatological conditions

The study period was warmer than the climatological mean of 5.6 °C (Drebs et al., 2002) with a temperature of 6.5 ± 8.7 °C (mean $\pm$ standard deviation, Fig. 2a). Year 2010 had a record cold winter and a record warm summer, with monthly means ranging from -10.7 °C (January) to 22.0 °C (July). The winters in 2008 and 2009, conversely, were mild and typical for Helsinki with near-average January temperatures of 0.2 °C and -3.2 °C. The number of snow-covered days for the three consecutive winters are 30, 81 and 112, with a mean albedo of 0.50 ± 0.11 (for times when global radiation

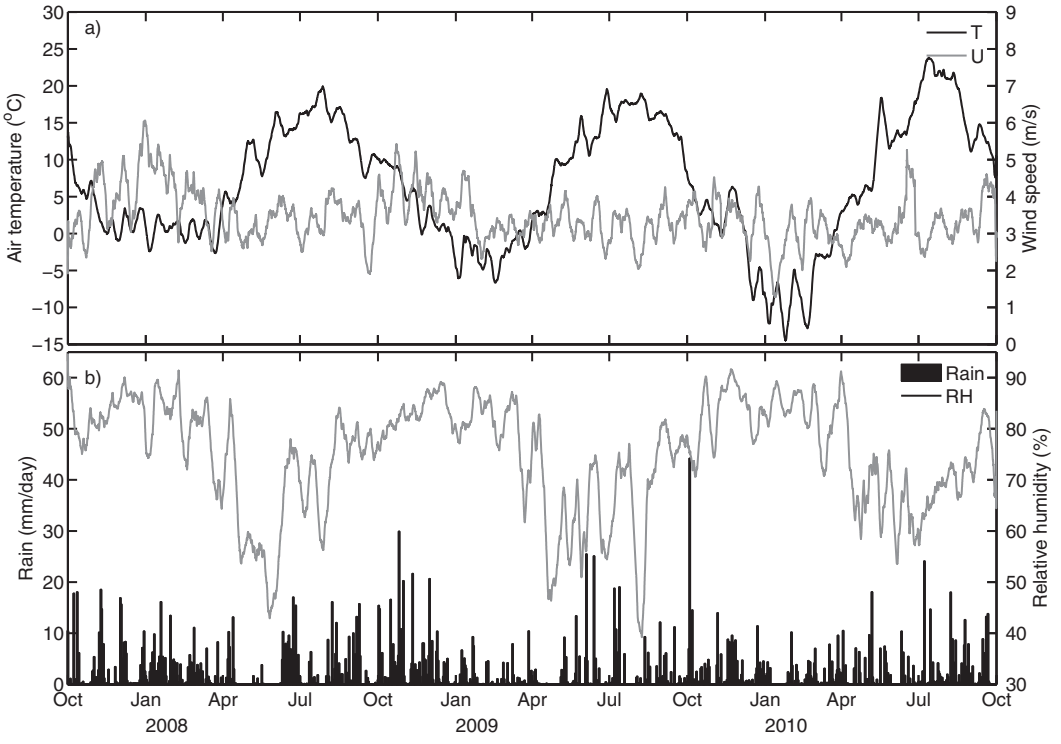

Fig. 2. (a) 5-d running means of air temperature (T, °C) and wind speed (U, ms^{-1}) at 31 m height. (b) Daily precipitation (mm d^{-1}) and 5-d running mean of relative humidity (RH,%).

input $>10\,\mathrm{W\,m^{-2}}$). The values are not dissimilar to the neighbourhood scale measurements at an urban site in Montreal (Bergeron and Strachan, 2010). Winter, spring and fall covered similar fractions of the measurement period to each other (with 22%, 20% and 20% occurrence) – whereas summer covered more, at 38% of the period. The mean wind speed at 31 m height was $3.4 \pm 1.6\,\mathrm{m\,s^{-1}}$ (Fig. 2a). South-west was the prevailing wind direction for all years, with a 20% occurrence. Furthermore, the relative humidity during the study period was $75.0 \pm 16.5\%$, which is 5% lower than the climatological mean (Fig. 2b). The annual precipitation sum, conversely, was 13% above the climatological mean with a value of $720\,\mathrm{mm\,yr^{-1}}$ (Fig. 2b).

3.2. Flux quality and error analysis

The detection limits and the random flux errors were calculated using quality-checked data from 2009 (Section 2.5), and the fluxes shown here and in the following two sections are calculated using the standard method combination. The mean detection limit for τ is $0.0414\,\mathrm{kg\,m^{-1}\,s^{-2}}$ and H $5.02\,\mathrm{W\,m^{-2}}$ (Table 3). The LE detection limits for closed- and open-path measurements are $4.73\,\mathrm{W\,m^{-2}}$ and $5.20\,\mathrm{W\,m^{-2}}$, and they do not deviate statistically significantly from each other ($p > 0.99$). The ratio of the detection limit to the observed flux is on average about 10% of the observed flux for all fluxes, which implies that the system is sensitive enough to measure the desired fluxes. To our knowledge, this type of detection limit has not been reported for any other urban site. The mean random uncertainties are close to the detection limits, and again the latent heat flux values do not deviate statistically significantly from each other. The random uncertainty – as percentages of the observed flux – is least for H (9.0%) and almost as good for τ (12.4%). The latent heat flux measurements are slightly more inaccurate, with random uncertainties of 16.1% and 15.8% for closed- and open-path measurements, respectively. The percentage values are close to those observed at vegetative sites (Finkelstein and Sims, 2001; Billesbach, 2011); no similar urban studies are available.

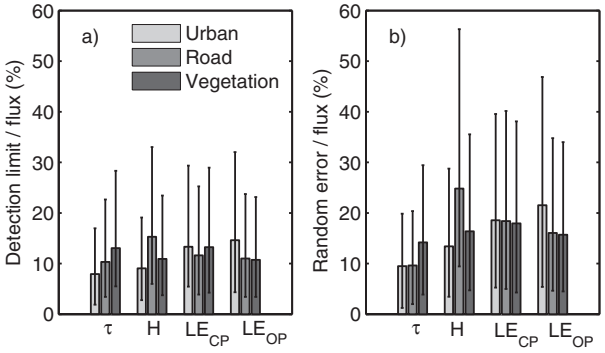

Fig. 3. (a) The ratio of the flux detection limit to the observed flux for momentum (τ), sensible heat (H) and closed- and open-path latent heat (LE_{CP}, LE_{OP}). Values are given for three wind direction sectors: urban (320–40°), road (40–180°) and vegetation (180–320°). Bars indicate means, and errorbars the 25th and 75th percentiles. (b) Same as (a) but for the ratio between the random flux error and the observed flux. Data are quality checked (as per text) and covers 2009.

The detection limit and random flux error, as percentages of the observed fluxes, for different wind direction sectors are shown in (Fig. 3). The momentum flux measurements are most reliable for the urban sector and worst for the vegetation sector according to both variables. The reason may be that the atmosphere is more unstably stratified in the urban sector, and the turbulence is better developed. The H measurements are also best for the urban sector and worst for the road sector, whereas the LE measurements perform best for the vegetation sector with strongest fluxes and are worst for the urban sector. All of the means for different sectors are within the 25th and 75th percentiles of the values of the other sectors.

3.3. Energy flux partitioning

Energy fluxes at the site vary largely through a year, over a day and with wind direction. Energy flux time series with half-an-hour flux values and 5-d running means of daily and nightly average fluxes are shown in Fig. 4. R_n, H and LE will be discussed here, whereas *Res* will be discussed in the following section. R_n ranges from -130

Table 3. Flux error analysis for momentum (τ), sensible heat (H) and closed- and open-path latent heat (LE_{CP}, LE_{OP}). Mean random flux error (units of flux), the ratio between the random flux error and the observed flux (%), the detection limit (units of flux) and the ratio between the detection limit and the observed flux (%) for all quality checked data in 2009.

	τ	H	LE_{CP}	LE_{OP}
Detection limit	$0.0414\,\mathrm{kg\,m^{-1}\,s^{-2}}$	$5.02\,\mathrm{W\,m^{-2}}$	$4.73\,\mathrm{W\,m^{-2}}$	$5.20\,\mathrm{W\,m^{-2}}$
Detection limit/flux	9.95%	10.60%	10.69%	10.81%
Random uncertainty	$0.0464\,\mathrm{kg\,m^{-1}\,s^{-2}}$	$6.39\,\mathrm{W\,m^{-2}}$	$6.70\,\mathrm{W\,m^{-2}}$	$7.63\,\mathrm{W\,m^{-2}}$
Random uncertainty/flux (%)	12.36%	9.05%	16.14%	15.75%

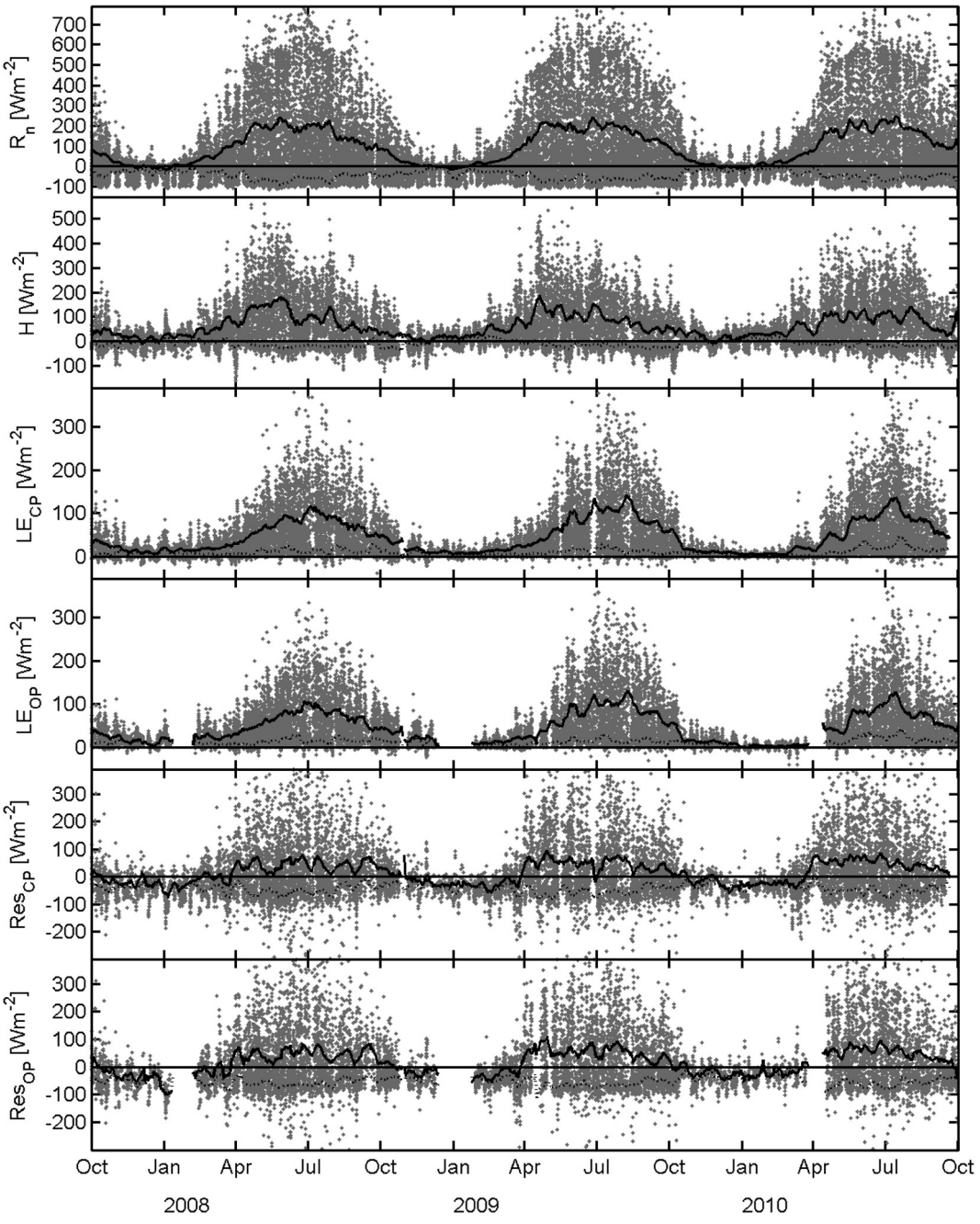

Fig. 4. Time series of net radiation (R_n), sensible heat flux (H), latent heat flux measured with a closed- and open-path analyser (LE_{CP}, LE_{OP}), and residuals of the energy balance (Res_{CP}, Res_{OP}), which is defined $Res = R_n - H - LE$. Grey dots indicate 30 min average fluxes, and the continuous and dashed lines are the 5-d running mean averages of day-time and night-time data, respectively. Turbulent flux data have been quality screened according to the text.

to $900\,W\,m^{-2}$, and the diurnal and seasonal patterns follow the solar angle. The 5-d running mean nocturnal R_n is negative throughout the year due to long-wave cooling and in summer it is lower than in winter due to higher surface temperatures. The day-time means range from $-16\,W\,m^{-2}$ in winter to $150\,W\,m^{-2}$ in mid-summer. H varies between $-190\,W\,m^{-2}$ and $560\,W\,m^{-2}$ being negative during night-time and in winter, indicating stable stratification. Similar behaviour was reported in Vesala et al. (2008). LE_{CP} and LE_{OP} vary between $-40\,W\,m^{-2}$ and $500\,W\,m^{-2}$, respectively. Negative fluxes are observed during 4.5% and 4.6% of occasions for LE_{CP} and LE_{OP},

respectively; and for over 80% of these occasions the wind is blowing from the vegetation sector where, anecdotally, dew formation is occasionally observed to develop. Furthermore, the open-path analyser underestimates LE by a few percent when compared with LE_{CP} ($LE_{CP} = 1.06\ LE_{OP} + 0$, $R^2 = 0.9762$, RMSE = 9.7766).

Energy flux partitioning generally differs for the various surface covers. Figure 5 shows the median diurnal cycles of energy fluxes normalised by the absolute value of R_n. The normalisation is done to minimise the effect of seasonal and synoptic variation, and cycles are presented for 20 degree wind segments. The upward flux is strongest in the urban sector throughout the day and in the traffic sector during morning and late afternoon rush hours (Fig. 5a). The vegetation sector has the weakest H, and no peaks are seen in the morning or afternoon. A slight heat island effect is seen in the urban and road sector since H is larger there during night compared with the vegetation sector. Latent heat flux, however, is largest when the wind is blowing from the direction with most forest and traffic ($160-220^\circ$, Fig. 5b and c). Morning peaks of latent heat are also seen during rush hour in the road sector but not elsewhere. The Bowen ratio (H/LE) varies strongly with wind direction, and the mean absolute value is smallest for the vegetation sector (0.37 ± 3.55), and almost the same for the urban sector (1.90 ± 3.77) and road sectors (1.65 ± 2.88). These results corroborate the findings reported in Vesala et al. (2008) for H and LE measured at the same site for the nine-month measurement period.

Furthermore, during snow cover, LE is largest in the urban and road sectors: this is perhaps consistent with enhanced winter-time evaporation caused by anthropogenic snow melting (not shown). A mean sublimation rate of $10\ W\ m^{-2}$ is seen for directions of vegetation. H is also observed to be double as large in the direction of buildings and roads in comparison with vegetative surfaces. For comparison, Lemonsu et al. (2008) observed that after snowmelt in springtime, Montreal's LE dropped to half of its share of R_n and the share of H increased by a third.

Our results can also be compared with those from mid-latitude urban flux sites since no other high-latitude urban measurements are yet available. Table 4 shows a summary of research on energy fluxes in cities located north of 45°N. Martin et al. (2009) showed average diurnal courses of H from campaigns at lower latitudes in London, Gothenburg, Edinburgh and Manchester and their values for weekdays vary between -20 and $+205\ W\ m^{-2}$, and Walsh et al. (2004) showed a range from 0 to $190\ W\ m^{-2}$ for a year of data from Vancouver. Bergeron and Strachan (2010) studied three sites during two winters in Montreal and had an average diurnal cycle of H peaking at $140\ W\ m^{-2}$ but their R_n input is $> 100\ W\ m^{-2}$ compared with Helsinki. Lemonsu et al. (2008) also reported a four-week spring campaign in Montreal, with H peaking at $200\ W\ m^{-2}$. Furthermore, Wood et al. (2010) reported that unstable stratification was three times as frequent as stable stratification in their 1.5 yr dataset at 190 m above London, which implies a mostly upward directed H. Vogt et al. (2006) also reported mostly positive H in summertime Basel, with peaks up to $400\ W\ m^{-2}$. Helfter et al. (2011), conversely, gave average diurnal courses of LE per season for a year of data from London (same site as Wood et al. above), with values ranging between 0 on an autumn night to $60\ W\ m^{-2}$ on a summer's day, which is about the same range as observed for Vancouver (Walsh et al., 2004). Furthermore, winter and spring time courses are observed to stay below $50\ W\ m^{-2}$ in Montreal (Lemonsu et al., 2008; Bergeron and Strachan, 2010) and LE is reported to generally be lower than $100\ W\ m^{-2}$ in Basel (Vogt et al., 2006). All in all, our results are in agreement with those from other urban sites when taking into account the high latitude and complex terrain.

3.4. Energy balance residual

The residual of the energy balance ranges from $-290\ W\ m^{-2}$ to $400\ W\ m^{-2}$, and the running mean nightly average for data from all wind directions is always negative indicating heat release from storage and/or an anthropogenic heat source (Fig. 4). The running mean daily averages are positive in summer, indicating that more heat is stored than is released from anthropogenic sources, whereas wintertime values are observed to be negative. The residual is smaller (i.e. more negative) in the urban sector implying the existence of an anthropogenic heat source (Fig. 5). Also, the morning and afternoon rush hours in the road sector appear more negative than the corresponding values in other sectors.

The overall magnitude of the energy balance residual is of the same order as observed at other urban sites (Grimmond and Oke, 1999; Christen and Vogt, 2004; Lemonsu et al., 2004; Bergeron and Strachan, 2010, Table 4). The annual variation in *Res* is larger, whereas the diurnal variation in winter is minimal compared with other sites; perhaps due to the northern latitude of Helsinki. Also, surface cover and population densities cause variation between sites. Q_F has been reported to vary between a few watts per square metre to even hundreds for small areas in Tokyo (Ichinose et al., 1999). Iamarino et al. (2011) estimated the annual mean anthropogenic heat flux for Greater London to be $11\ W\ m^{-2}$ in their extensive study. The only urban wintertime study is from Montreal, where an average Q_F of $35\ W\ m^{-2}$ was observed for an urban site and $10\ W\ m^{-2}$ for a suburban site (Bergeron and Strachan, 2010). The closest studied cities in terms of latitude are Fairbanks and Reykjavik, where the average Q_F is reported

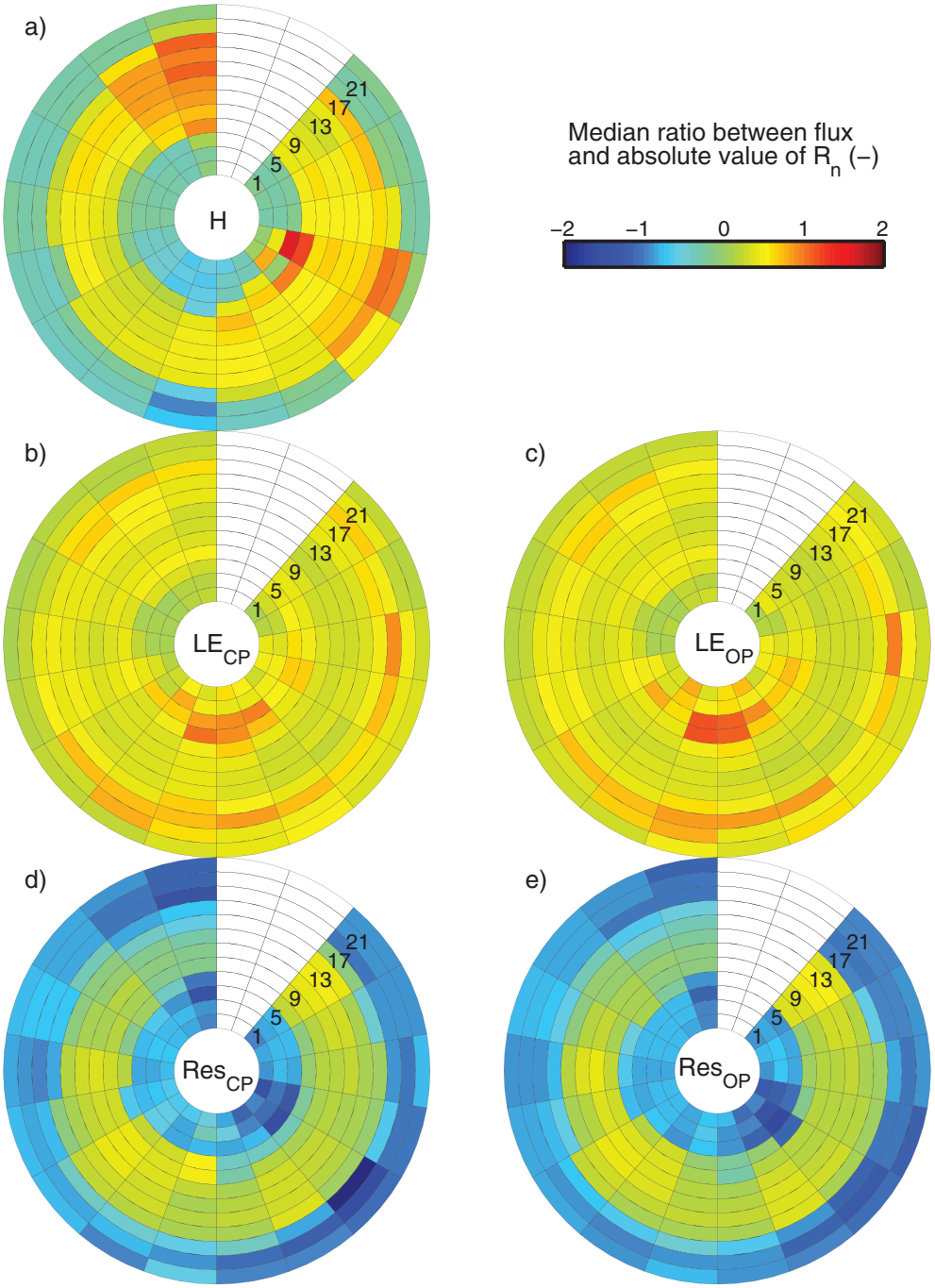

Fig. 5. Average diurnal cycles for 20 degree wind direction sectors. Hours are labelled with 2-hour resolution and run from 1:00 (local time) closest to the centre to 23:00 (local time) on the outside of the subplots. Colours indicate the median of the energy flux divided by the absolute value of net radiation (R_n); see colourbar. The energy fluxes are (a) sensible heat flux (H), (b) closed-path latent heat flux (LE_{CP}), (c) open-path latent heat flux (LE_{OP}), (d) residual of the energy balance using LE_{CP} and (e) residual of the energy balance using LE_{OP}. All turbulent fluxes have been quality checked (see text), ratios exceeding 10 have been omitted from the plot, and data cover the whole period from October 2007 to September 2010 inclusive.

to be $6\,W\,m^{-2}$ (Oke, 1988) and $35\,W\,m^{-2}$ (Steinecke, 1999). The latter also gives $13\,W\,m^{-2}$ for vehicular emissions, which is close to the morning and afternoon rush hour values given by Grimmond (1992) and Bergeron and Strachan (2010). Using characteristic values from Sailor (2011) and a morning rush hour traffic rate of

Table 4. Heat fluxes in cities with a cold temperate climate (latitude >45°N). The ranges of mean diurnal courses are given for the sensible (H) and latent (LE) heat fluxes, the energy balance residual ($Res = R_n - H - LE = \Delta Q_S - Q_F$) in addition to the anthropogenic heat flux (Q_F).

Reference	City	Latitude (°N)	Data period and season	H (W m^{-2})	LE (W m^{-2})	Res (W m^{-2})	Q_F (W m^{-2})
Oke (1988)	Moscow	55.750	1 yr	–	–	–	127[a]
	Montreal	45.503					99
	Vancouver	49.291					19
	Fairbanks	64.849					6
Grimmond and Oke (1999)	Vancouver, industr.	49.267	1 month fall, 3 months summer	69[b]	17[b]	−200–400[c]	–
	Vancouver, suburb.	49.250		84	31	−80–250	
Walsh et al. (2004)	Vancouver	49.226	1 yr	0–190	−5–50	–	–
Lemonsu et al. (2008)	Montreal	45.503	4 weeks spring	0–200	0–50	−100–330	–
Bergeron and Strachan (2010)	Montreal, rural	45.547	2 winters	−10–25	0–35	−30–80	–
	Montreal, suburb.	45.501		−5–130	0–35	−60–140	7–13[d]
	Montreal, urban	45.328		0–140	0–20	−50–145	25–45
Steinecke (1999)	Reykjavik	64.134	1 yr	–	–	–	35[a]
Christen and Vogt, 2004	Basel, urban 1	47.556	1 month summer	10–250	0–90	–100–200	20[e]
	Basel, urban 2	47.552		0–250	0–100	−80–200	10
	Basel, urban 3	47.555		−10–200	0–40	−80–130	20
	Basel, suburban	47.552		−5–180	5–150	−100–180	5
Vogt et al. (2006)	Basel	47.556	1 month summer	−20–400[c]	0–100[c]	–	–
Offerle et al. (2005)	Łódź	51.767	2 yr	−5–200	10–105	−100–180[f]	−30–50[f]
Mårtensson et al. (2006)	Stockholm	59.303	49 d spring	27.7[g]	–	–	–
Martin et al. (2009)	London	51.518	~1 month campaigns, different seasons	−20–125	–	–	–
	Gothenburg	57.700		−5–60			
	Edinburgh	55.950		−25–170			
	Manchester	53.483		−10–205			
Helfter et al. (2011)	London	51. 518	1 yr	–	0–60[h]	–	–
Iamarino et al. (2011)	Greater London	51.500	4 yr	–	–	–	11[a]
Current study	Helsinki	60.210	3 yr	−17–125	11–95[I] 10–88	−62–89[I] −53–69	13[e]

[a]Annual means obtained by summing up contributions of human metabolism, vehicular traffic and buildings, using, e.g., energy consumption and population statistics.
[b]Daily means.
[c]Individual values.
[d]Same as footnote 'a' but for the range of values in a diurnal course.
[e]Annual average estimated assuming that ΔQ_S has to be zero over a year.
[f]ΔQ_S is obtained using the Element surface temperature method, where element surface temperatures are measured and the heat transfer through the elements are modelled. $Q_F = H + LE + \Delta Q_S - R_n$.
[g]Mean of the whole period.
[h]Range is from autumn night to summer day.
[i]Values for open-path and closed-path gas analysers.

3000 vehicles per hour at the road close to our tower, H and LE can be estimated to be $21\,W\,m^{-2}$ and $10\,W\,m^{-2}$ from the traffic on the road. The average fluxes from the road sector during weekday rush hours for times with snow cover are $23\,W\,m^{-2}$ for H and $8\,W\,m^{-2}$ for LE, which correspond well with the estimates. Only fluxes over snow cover are used in the comparison to ensure that the fluxes represent the road as snow cover has minimised evapotranspiration. For comparison, Sailor and Lu (2004) reported anthropogenic heating as much as $300\,W\,m^{-2}$ during afternoon rush hours over a vehicle sector.

3.5. *Differences in fluxes between calculation types*

The effects of different calculation procedures on the turbulent fluxes are shown in Fig. 6 and discussed in the following section.

3.5.1. Spectral corrections. Leaving out the spectral corrections is not acceptable since it causes a 4.6% underestimation for τ, 3.2% for H, 5.1% for LE_{OP} and as much as 26.2% for LE_{CP}. For comparison Christen and Vogt (2004) showed that spectral corrections of H in Basel were below 1% and ranged from 2 to 7% for LE_{OP}. However, they did not include the low-frequency spectral correction (TF_{LF} in eq. 8), which in our case accounts for almost all spectral correction of τ and H, and 3 percentage points of the correction of LE_{OP} and LE_{CP}. Using a theoretical TF_{HF}, which does not take into account high-frequency RH effects for LE_{CP}, would still cause a 22.0% underestimation since a strong dependency of response time (t_{H_2O}) on RH was observed (not shown). The mean t_{H_2O} ranges from 1.0 s at 40% RH to 7.1 s for 80% RH. Mammarella et al. (2009) found a similar RH dependency where t_{H_2O} varied between 0.3 s and 2.5 s for a 7 m length of dirty tube, whereas Ibrom et al. (2007) got a range from 2.3 s to 8.8 s for their 50 m tube. Interestingly, the H values are also affected by alterations in LE_{CP} through the sonic heat correction, but the effect is less than a percent. All underestimations are larger in stable than unstable stratification since smaller turbulence becomes more dominant as stability increases and TF_{HF} increases (Fig. 6).

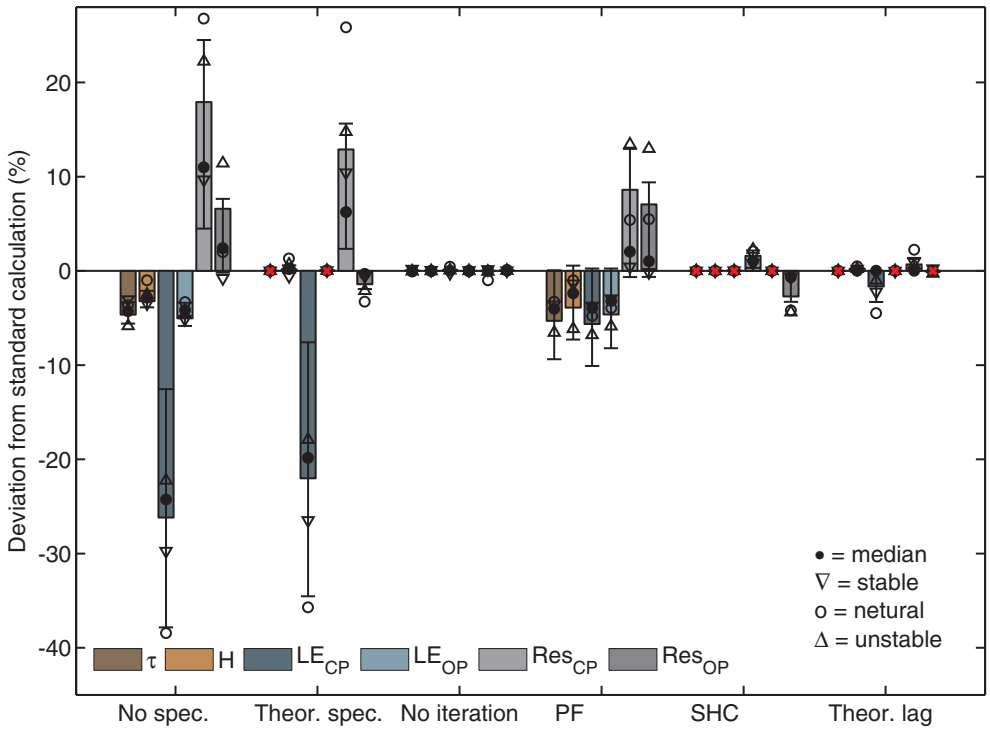

Fig. 6. Calculation procedure effects on turbulent flux magnitudes for momentum (τ), sensible heat (H) and closed- and open-path latent heat (LE_{CP}, LE_{OP}), in addition to effects on energy balance residuals (Res_{CP}, Res_{OP}). Bars give the means over all stabilities; and means for different stability classes are denoted by ∇ (stable, $\zeta > 0.01$), o (neutral, $-0.01 < \zeta < 0.01$), Δ (unstable, $\zeta < -0.01$). Errorbars denote 25th and 75th percentiles, and the median is denoted by a filled circle (●). Red crosses show fluxes that are not affected by a certain calculation procedure. Deviations are calculated as (flux-flux$_{Standard}$) flux$^{-1}_{Standard}$ except for *Res* where an absolute value of the denominator is used since corrections can easily change the sign of *Res*.

3.5.2. Iteration. This was needed (flux change >1%) in 22% of all cases, and almost all (95%) of these situations were characterised by stable stratification. The reason for this is that the spectral peak frequency increases with stability (i.e. the co-spectrum is shifted to higher frequencies), and thus TF_{HF} grows and the fluxes are increased. Nevertheless, the average effect of iteration stays below one percent even though noise is introduced into data (Fig. 6). Mauder et al. (2008) reported that half of the EC data post-processing software used in CarboEurtope include iteration but the resulting effect on final flux values is not given. Mauder and Foken (2006), on the other hand, noted that their LE_{OP} was affected by 0.3% and H by 1.5% by the inclusion of an iteration loop.

3.5.3. Planar fitting. The fluxes obtained using planar fitting are on average smaller (Fig. 6, τ 5.3%, H 3.9%, LE_{OP} 4.6%, LE_{CP} 5.7%) than with a 2-D rotation as in Vesala et al. (2008). The underestimation is about 3% points larger for unstable situations compared with stable and neutral stratification for all fluxes, which implies that the streamlines are heavily affected by stability. Differences depend also on wind direction and underestimations of 6%, for all fluxes are observed when the wind is blowing from the sloping terrain to the South (150–210°), and all mean underestimations exceed 10% for north-westerly winds (320–360°). Similar insufficiency of the planar fitting method has also been seen for complex mountainous forest sites (Göckede et al., 2008). Burns et al. (2011) also showed that planar fitting is prone to errors stemming from stability effects in sloping terrain. The flux quality (Section 3.2), on the other hand, did not change statistically significantly when using the planar fitting method as opposed to 2-D rotation.

3.5.4. Surface heating correction of LE_{OP}. The surface heating correction increases E_{OP} on average by 1.6% (Fig. 6), and the slope between LE_{OP} and LE_{CP} decreases from 1.06 to 1.04 (not shown). The correction is the same for both the period from which the parameterisations (eq. 9) were obtained and for the independent period before that. The measured analyser surface was always warmer than the air ($T_s - T_a > 0$), and the mean temperature difference was 3.1 ± 5.2 °C. For comparison, the open-path CO_2 flux increased by 2.5%, whereas Järvi et al. (2009a) gave a 4% increase with a similar method, which was further developed in this paper. Furthermore, Burba and Anderson (2010) noted that the correction is usually only important for CO_2 in extremely cold conditions.

3.5.5. Lag time and cross-correlation functions of LE_{CP}. The lag time of closed-path H_2O measurements is observed to depend strongly on RH. Figure 7 shows an example with data from May and June 2010. The fit approaches 39.9 s when RH goes to 100% and 7.1 s when RH goes to 0%. The latter coincides with the theoretical lag time and is close to the observed lag time for CO_2 measurements

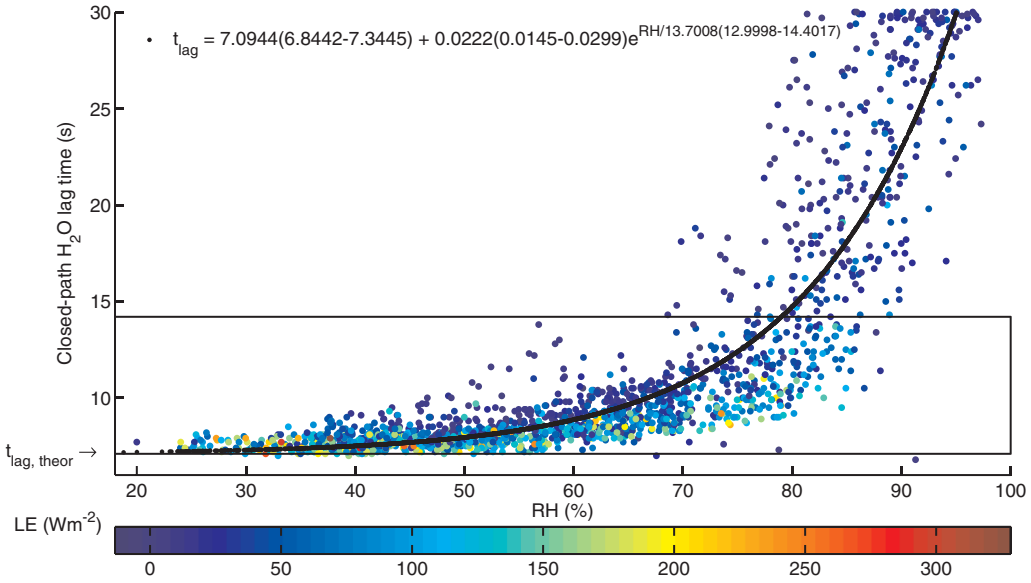

Fig. 7. Lag time (s) of closed-path H_2O measurements as a function of relative humidity (%) and an exponential with 95% confidence intervals. The theoretical lag time ($t_{lag,theor}$) and the theoretical lag window (rectangle) are also given. The colourbar gives the latent heat flux magnitude (LE, W m^{-2}). Data are from May and June 2010.

(of 7.4 s). When the theoretical lag window (rectangle in Fig. 7) is used, LE_{CP} is on average 1.8% smaller. The difference is small but logical, considering that the weakest fluxes are observed with high *RH*. Furthermore, using a theoretical lag window results in 15% less data compared with using our improved method. In the method, a larger lag window is used when trying to find t_{lag}, and if t_{lag} is not found, the lag time is retrieved from the exponential fit (Fig. 7). The cases when the lag was not found despite a larger window cover 5.8% of the dataset and have a mean *RH* of 84%. Water vapour tube effects are widely studied in terms of spectral corrections but less attention is given to the lag time optimisation. Clement (2004) found a similar relative humidity dependency for their 18 m tube, with lag times ranging approximately from 7 to 25 s.

In addition to the increase in lag time, the shapes of the water vapour cross-correlation functions also depend on relative humidity. Figure 8 shows means and standard deviations for normalised cross-correlation function for data in September 2009. Generally, when small-scale turbulence is attenuated in the tube leading to the analyser, the peak of the cross-correlation function is not that sharp. Furthermore, the slope at which the cross-correlation function falls around the peak is always as sharp when q' is leading w' ($t > 0$ in Fig. 8), but the slope decreases with *RH* when q' is lagging w'. This is due to the adsorption and desorption processes in the tube, which lengthen the time it takes for the water vapour signal to travel down the sampling tube.

3.5.6. Flux averaging period. The flux averaging period was studied using Ogive analysis, and (Fig. 9) shows the occurrence of convergent Ogives and those that have a maximum before converging. Non-convergent Ogives are not observed in the quality-checked data, and only classes (1) and (2) in Section 2.4.2 are present. The momentum Ogives converge within 30 min in 71% of the cases, whereas *H*, LE_{CP} and LE_{CP} converge in 85%, 93% and 89% of the time, respectively. The discrepancy is explained by the fact that momentum is transported by larger eddies than scalars are (e.g. Kaimal and Finnigan, 1994). The Ogive convergence did not have a seasonal or diurnal pattern.

The choice of flux averaging period on the final flux values was also studied. Usually, when the averaging period is decreased, the flux also decreases since large-scale turbulence is not taken into account. At the same time, though, the low-frequency spectral correction (TF_{LF}, eq. 8) increases the flux as a function of averaging period. The increase ranges from about 15% for 5 min averaging to 2% for 60 min averaging. The outcome is that the modes of deviations from 30 min-averaged fluxes show a 5% overestimation of fluxes when using a 5 min averaging period and a similar underestimation for 60 min averaging. Furthermore, 5 and 60 min averaging cause a random uncertainty of about 6% and 8%, respectively.

3.6. *Calculation procedure effect on energy balance residual*

The monthly average residual of the energy balance is usually positive only from April to July (Fig. 10a), and the annual means are $-12.7\,W\,m^{-2}$ and $-13.9\,W\,m^{-2}$ for open- and closed-path measurements, respectively. Since

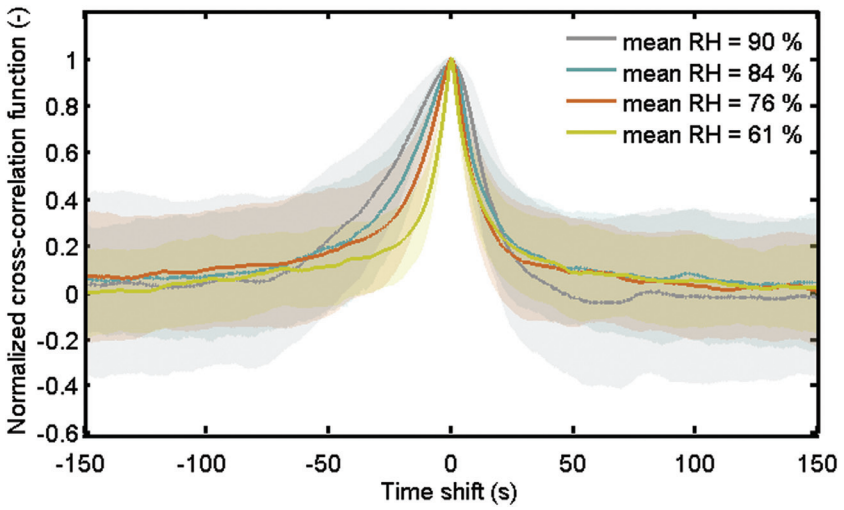

Fig. 8. Normalised cross-correlation functions of closed-path H_2O measurements as a function of time shift (s) for different relative humidities. The time lag has been taken into account and negative time shifts correspond to H_2O signal lagging the vertical wind speed signal. Thick lines are means and shaded patches are standard deviations. Data are from September 2009.

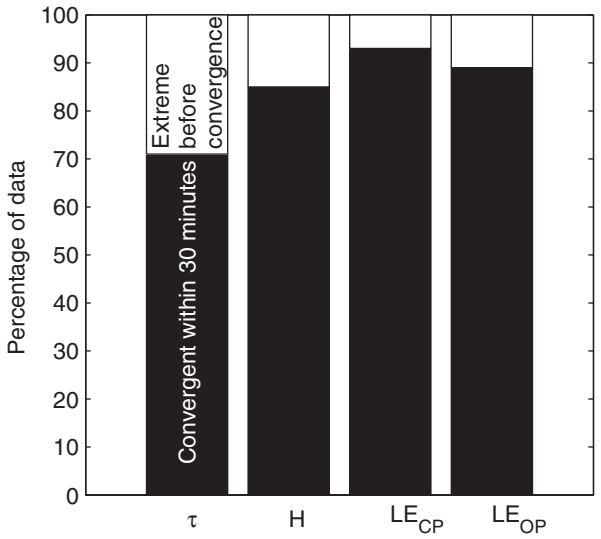

Fig. 9. Flux convergence for momentum (τ), sensible heat (H) and closed- and open-path latent heat (LE_{CP}, LE_{OP}). Proportion of flux Ogives that converge within a 30 min averaging period (black) or have an extreme value before converging within 219 min (white). No quality-checked data fell into the class of non-convergent Ogives.

the change in heat storage should be near zero over the course of a year, these mean residuals can be attributed to anthropogenic heat release (Table 4). The discrepancy between fluxes gained with different EC data post-processing can be even greater than the average residual (Fig. 10b and c). Omitting the spectral correction always overestimated Res_{CP} because both H and LE_{CP} are underestimated, and the overestimation can be up to $14\,W\,m^{-2}$ with an average of 17.9% (Fig. 6). Also, applying only the theoretical spectral correction for LE_{CP} overestimates Res_{CP} by up to $9\,W\,m^{-2}$ or 12.9% on average. Res_{OP}, conversely, is overestimated (12.9%) when spectral corrections are not applied and underestimated (1.4%) when a theoretical spectral correction to LE_{CP} is made. Planar fitting leads to an overestimation of Res_{CP} and Res_{CP} as would be expected. The surface heating correction underestimates Res_{OP} by 2.7% if the correction is left undone: the effect ranges from almost zero in winter to $2\,W\,m^{-2}$ during summer when there is a higher global radiation input. Likewise, using a theoretical lag window only concerns LE_{CP}, and Res_{CP} is overestimated only by 0.7% if the correction is left out.

4. Conclusions

We presented data from three consecutive years from the world's northernmost urban flux measurement station. The turbulent fluxes of sensible and latent heat exhibited substantial seasonal and diurnal variation in addition to a surface cover dependency. The annual mean residual of the energy balance suggests an average anthropogenic heat source of about $13\,W\,m^{-2}$, with distinct contributions from traffic during rush hours. Furthermore, anthropogenic snowmelt might increase evaporation during winter.

We tested the effect of various alterations in raw EC data post-processing, the key recommendations are as follows:

- The detection limits of fluxes should be reported, especially at urban sites with low evaporation when the fluxes are often close to their detection limit.
- The calculation of random uncertainties should be performed, especially in relation to model performance evaluation.
- Special attention should be paid to water vapour interaction with tube walls, which affects closed-path LE measurements, since using a too small lag window can cause a 15% lack of data, and leaving out spectral corrections a 26% underestimation of LE.
- The surface heating correction of LE_{OP} is less crucial ($<2\%$ overestimation) as that of CO_2.
- Using planar fitting in complex sites is prone to errors stemming from the dependency of flow streamlines on stability, and thus should be applied with caution.
- The inclusion of iteration when performing corrections does not improve the flux much ($<1\%$), but the procedure should be included in flux calculation codes since it is sound and not laborious to implement.
- The effect of changes in EC flux-calculation procedures on the energy balance residual can be larger than the residual itself. Leaving out spectral corrections, for instance, overestimates Res_{OP} by 13% and Res_{CP} by 18%.

Most of our results are specific to our measurement setup, but the results can be interpreted as an example and a warning for anyone performing EC measurements. Special caution should be made at urban flux sites – where the residual of the energy balance is often interpreted as the change in heat storage or anthropogenic heat release – since the order of magnitude of the residual is close to that of potential systematic errors in flux calculations. Nevertheless, a balance between the laborious, but conductive, do-it-yourself approach and global uniform EC data post-processing should be strived for.

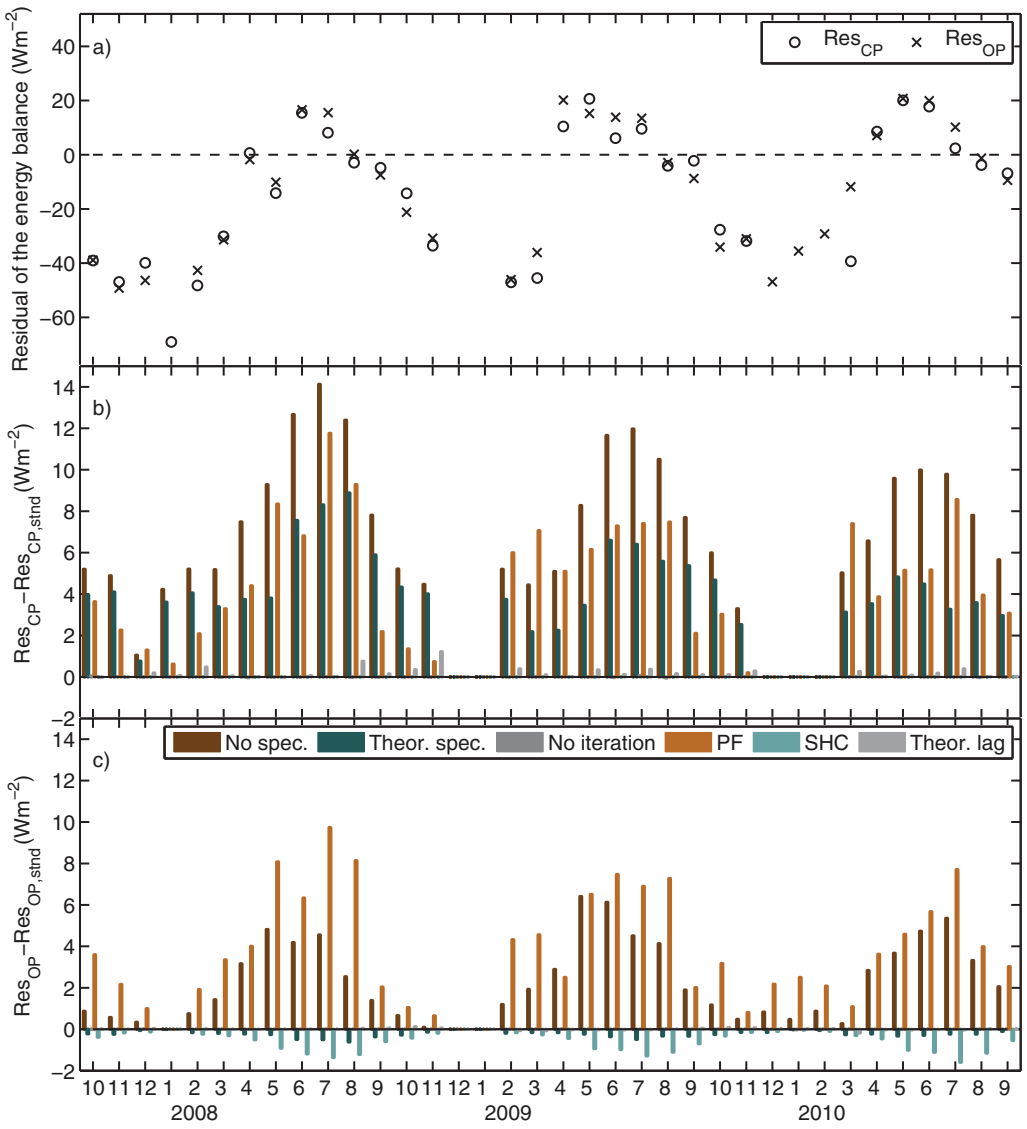

Fig. 10. (a) Monthly mean residual of the surface energy balance (W m^{-2}, eq. 2) with closed-path (Res_{CP}) and open-path (Res_{OP}) analyser evaporation, (b) difference between a modified Res_{CP} and the standard Res_{CP}, (c) same for Res_{OP}. Values in (b) and (c) are given for different calculation procedures: no spectral correction, theoretical spectral correction of LE_{CP}, no iteration, planar fitting, surface heat correction of LE_{OP} and theoretical lag time of LE_{CP}. Only times when the data for all calculation types are available are included, and some months are thus omitted due to a lack of data. See text for further details.

5. Acknowledgements

For funding we thank the Academy of Finland Centre of Excellence program (project no 1118615) and the Academy of Finland project 138328. Also the EU-funded projects BRIDGE, IMECC and ICOS and Tekes project Ubicasting are gratefully thanked. We also thank Ivan Mammarella, Erkki Siivola, Petri Keronen, Samuli Launiainen for the help during the study.

References

Aubinet, M., Grelle, A., Ibrom, A., Rannik, Ü., Moncrieff, J. and co-authors. 2000. Estimates of the annual net carbon and water exchange of forests: the EUROFLUX methodology. *Adv. Ecol. Res.* **30**, 113–175.

Bergeron, O. and Strachan, I. B. 2010. Wintertime radiation and energy budget along an urbanization gradient in Montreal, Canada. *Int. J. Climatol.* Online Library, 1–16.

Best, M. J. 2005. Representing urban areas within operational numerical weather prediction models. *Bound. -Layer Meteorol* **114**, 91–109.

Billesbach, D. P. 2011. Estimating uncertainties in individual eddy covariance flux measurements: a comparison of methods and a proposed new method. *Agric. For. Meteorol.* **151**, 394–405.

Burba, G. and Anderson, D. 2010. A brief practical guide to eddy covariance flux measurements. *LI-COR Biosci.*, 1–212. http://www.licor.com/env/applications/eddy_covariance/book.html

Burba, G. G., McDermitt, D. K., Grelle, A., Anderson, D. J. and Xu, L. 2008. Addressing the influence of instrument surface heat exchange on the measurements of CO_2 flux from open-path gas analyzers. *Global Change Biol.* **14**, 1854–1876.

Burns, S. P., Sun, J., Lenschow, D. H., Oncley, S. P., Stephens, B. B. and co-authors. 2011. Atmospheric stability effects on wind fields and scalar mixing within and just above a Subalpine forest in sloping terrain. *Bound. -Layer Meteorol.* **138**, 231–262.

Christen, A. and Vogt, R. 2004. Energy and radiation balance of a central European city. *Int. J. Climatol.* **24**, 1395–1421.

Clement, R. 2004. *Mass and Energy Exchange Of A Plantation Forest In Scotland Using Micrometeorological Methods, Chapter 5*. PhD Dissertation, University of Edinburgh, UK. http://www.geos.ed.ac.uk/homes/rclement/PHD/

Drebs, A., Nordlund, A., Karlsson, P., Helminen, J. and Rissanen, P. 2002. *Tilastoja Suomen ilmastosta 1971–2000* [Climatological Statistics of Finland 1971–2000]. Finnish Meteorological Institute, Finland.

EEA, 2006. Urban sprawl in Europe – the ignored challenge. *Europe. Env. Agency*. **10**, 1–60.

Finkelstein, P. L. and Sims, P. F. 2001. Sampling error in eddy correlation flux measurements. *J. Geophys. Res. Atmos.* **106**, 3503–3509.

Finnigan, J. J., Clement, R., Malhi, Y., Leuning, R. and Cleugh, H. A. 2003. A re-evaluation of long-term flux measurement techniques – part I: averaging and coordinate rotation. *Bound. -Layer Meteorol.* **107**, 1–48.

Foken, T. and Wichura, B. 1996. Tools for quality assessment of surface-based flux measurements. *Agric. For. Meteorol.* **78**, 83–105.

Foken, T., Wimmer, F., Mauder, M., Thomas, C. and Liebethal, C. 2006. Some aspects of the energy balance closure problem. *Atmos. Chem. Phys.* **6**, 4395–4402.

Frey, C. M., Parlow, E., Vogt, R., Harhash, M. and Wahab, M. M. A. 2011. Flux measurements in Cairo. Part 1: in situ measurements and their applicability for comparison with satellite data. *Int. J. Climatol.* **31**, 218–231.

Göckede, M., Foken, T., Aubinet, M., Aurela, M., Banza, J. and co-authors. 2008. Quality control of CarboEurope flux data – part 1: coupling footprint analyses with flux data quality assessment to evaluate sites in forest ecosystems. *Biogeosciences*. **5**, 433–450.

Grelle, A. and Burba, G. 2007. Fine-wire thermometer to correct CO_2 fluxes by open-path analyzers for artificial density fluctuations. *Agric. For. Meteorol.* **147**, 48–57.

Grimmond, C. S. B. 1992. The suburban energy-balance – methodological considerations and results for a midlatitude west-coast city under winter and spring conditions. *Int. J. Climatol.* **12**, 481–497.

Grimmond, C. S. B., Blackett, M., Best, M. J., Baik, J., Belcher, S. E. and co-authors. 2011. Initial results from Phase 2 of the international urban energy balance model comparison. *Int. J. Climatol.* **31**, 244–272.

Grimmond, C. S. B., Blackett, M., Best, M. J., Barlow, J., Baik, J. and co-authors. 2010. The International urban energy balance models comparison project: first results from phase 1. *J. Appl. Meteorol. Climatol.* **49**, 1268–1292.

Grimmond, C. S. B. and Oke, T. R. 1999. Heat storage in urban areas: local-scale observations and evaluation of a simple model. *J. Appl. Meteorol.* **38**, 922–940.

Grimmond, C. S. B., Salmond, J. A., Oke, T. R., Offerle, B. and Lemonsu, A. 2004. Flux and turbulence measurements at a densely built-up site in Marseille: heat, mass (water and carbon dioxide), and momentum. *J. Geophys. Res. Atmos.* **109**, D24101.

He, H., Liu, M., Sun, X., Zhang, L., Luo, Y. and co-authors. 2010. Uncertainty analysis of eddy flux measurements in typical ecosystems of ChinaFLUX. *Ecol. Inform.* **5**, 492–502.

Helfter, C., Famulari, D., Phillips, G. J., Barlow, J. F., Wood, C. R. and co-authors. 2011. Controls of carbon dioxide concentrations and fluxes above central London. *Atmos. Chem. Phys.* **11**, 1913–1928.

Hollinger, D. Y. and Richardson, A. D. 2005. Uncertainty in eddy covariance measurements and its application to physiological models. *Tree Physiol.* **25**, 873–885.

Horst, T. W. 1997. A simple formula for attenuation of eddy fluxes measured with first-order-response scalar sensors. *Bound. -Layer Meteorol.* **82**, 219–233.

Horst, T. W. 2000. On frequency response corrections for eddy covariance flux measurements. *Bound. -Layer Meteorol.* **94**, 517–520.

Iamarino, M., Beevers, S. and Grimmond, C. S. B. 2011. High-resolution (space, time) anthropogenic heat emissions: London 1970–2025. *Int. J. Climatol.* In press.

Ibrom, A., Dellwik, E., Flyvbjerg, H., Jensen, N. O. and Pilegaard, K. 2007. Strong low-pass filtering effects on water vapour flux measurements with closed-path eddy correlation systems. *Agric. For. Meteorol.* **147**, 140–156.

Ichinose, T., Shimodozono, K. and Hanaki, K. 1999. Impact of anthropogenic heat on urban climate in Tokyo. *Atmos. Environ.* **33**, 3897–3909.

Järvi, L., Hannuniemi, H., Hussein, T., Junninen, H., Aalto, P. P. and co-authors. 2009b. The urban measurement station SMEAR III: continuous monitoring of air pollution and surface-atmosphere interactions in Helsinki, Finland. *Boreal Environ. Res.* **14**, 86–109.

Järvi, L., Mammarella, I., Eugster, W., Ibrom, A., Siivola, E. and co-authors. 2009a. Comparison of net CO2 fluxes measured with open- and closed-path infrared gas analyzers in an urban complex environment. *Boreal Environ. Res.* **14**, 499–514.

Kaimal, J. C. and Finnigan, J. J. 1994. *Atmospheric Boundary Layer Flows, Their Structure And Measurements*. Oxford University Press, New York, p. 289.

Koskinen, J. T., Poutiainen, J., Schultz, D. M., Joffre, S., Koistinen, J. and co-authors. 2011. THE HELSINKI

TESTBED: a mesoscale measurement, research, and service platform. *Bull. Am. Meteorol. Soc*. **92**, 325–342.

Launiainen, S. 2010. Seasonal and inter-annual variability of energy exchange above a boreal Scots pine forest. *Biosci*. **7**, 1–20.

Lemonsu, A., Belair, S., Mailhot, J., Benjamin, M., Chagnon, F. and co-authors. 2008. Overview and first results of the Montreal urban snow experiment 2005. *J. Appl. Meteorol. Climatol*. **47**, 59–75.

Lemonsu, A., Grimmond, C. S. B. and Masson, V. 2004. Modeling the surface energy balance of the core of an old Mediterranean city: Marseille. *J. Appl. Meteorol*. **43**, 312–327.

Lenschow, D. H., Mann, J. and Kristensen, L. 1994. How long is long enough when measuring fluxes and other turbulence statistics. *J. Atmos. Ocean. Technol*. **11**, 661–673.

Leuning, R. and Judd, M. J. 1996. The relative merits of open- and closed-path analyzers for measurements of eddy fluxes. *Global Change Biol*. **2**, 241–253.

Liu, H. P., Peters, G. and Foken, T. 2001. New equations for sonic temperature variance and buoyancy heat flux with an omnidirectional sonic anemometer. *Bound. -Layer Meteorol*. **100**, 459–468.

Mahrt, L., Sun, J., Blumen, W., Delany, T. and Oncley, S. 1998. Nocturnal boundary-layer regimes. *Bound. Layer Meteorol*. **88**, 255–278.

Mammarella, I., Launiainen, S., Gronholm, T., Keronen, P., Pumpanen, J. and co-authors. 2009. Relative humidity effect on the high-frequency attenuation of water vapor flux measured by a closed-path eddy covariance system. *J. Atmos. Ocean. Technol*. **26**, 1856–1866.

Mårtensson, E. M., Nilsson, E. D., Buzorius, G. and Johansson, C. 2006. Eddy covariance measurements and parameterisation of traffic related particle emissions in an urban environment. *Atmos. Chem. Phys*. **6**, 769–785.

Martin, C. L., Longley, I. D., Dorsey, J. R., Thomas, R. M., Gallagher, M. W. and co-authors. 2009. Comparing urban particle emission fluxes measured on the BT Tower (London) with measurements from Manchester, Edinburgh and Gothenburg. *Inhaled Particles, X*, 151.

Massman, W. J. 2001. Reply to comment by Rannik on ''A simple method for estimating frequency response corrections for eddy covariance systems''. *Agric. For. Meteorol*. **107**, 247–251.

Massman, W. J. 2000. A simple method for estimating frequency response corrections for eddy covariance systems. *Agric. For. Meteorol*. **104**, 185–198.

Massman, W. J. and Ibrom, A. 2008. Attenuation of concentration fluctuations of water vapor and other trace gases in turbulent tube flow. *Atmos. Chem. Phys*. **8**, 6245–6259.

Mauder, M., Foken, T., Clement, R., Elbers, J. A., Eugster, W. and co-authors. 2008. Quality control of CarboEurope flux data – part 2: inter-comparison of eddy-covariance software. *Biogeosciences*. **5**, 451–462.

Mauder, M., Oncley, S. P., Vogt, R., Weidinger, T., Ribeiro, L. and co-authors. 2007. The energy balance experiment EBEX-2000. Part II: inter-comparison of eddy-covariance sensors and post-field data processing methods. *Bound. -Layer Meteorol*. **123**, 29–54.

Mauder, M. and Foken, T. 2006. Impact of post-field data processing on eddy covariance flux estimates and energy balance closure. *Meteorol. Z*. **15**, 597–609.

Moncrieff, J., Clement, R., Finnigan, J. and Meyers, T. 2004. Averaging, detrending, and filtering of eddy covariance time series. In: *Handbook of Micrometeorology: A guide for Surface Flux Measurement and Analysis* (eds X. Lee, W. Massman, B. Law, X. Lee, W. Massman, and B. Law). Kluwer Academic Publishers, the Netherlands, pp. 7–31.

Moncrieff, J., Massheder, J. M., de Bruin, H., Elbers, J., Friborg, T. and co-authors. 1997. A system to measure surface fluxes of momentum, sensible heat, water vapour and carbon dioxide. *J. Hyrdrol*. **188–189**, 589–611.

Moore, C. J. 1986. Frequency response corrections for eddy correlation systems. *Bound. -Layer Meteorol*. **37**, 17–35.

Moriwaki, R. and Kanda, M. 2006. Local and global similarity in turbulent transfer of heat, water vapour, and CO2 in the dynamic convective sublayer over a suburban area. *Bound. -Layer Meteorol*. **120**, 163–179.

Nemitz, E., Hargreaves, K. J., McDonald, A. G., Dorsey, J. R. and Fowler, D. 2002. Micrometeorological measurements of the urban heat budget and CO_2 emissions on a city scale. *Environ. Sci. Technol*. **36**, 3139–3146.

Nordbo, A., Launiainen, S., Mammarella, I., Leppäranta, M., Huotari, J. and co-authors. 2011. Long-term energy flux measurements and energy balance over a small boreal lake using eddy covariance technique. *J. Geophys. Res*. **116**, 1–17.

Offerle, B., Grimmond, C. S. B. and Fortuniak, K. 2005. Heat storage and anthropogenic heat flux in relation to the energy balance of a central European city centre. *Int. J. Climatol*. **25**, 1405–1419.

Offerle, B., Grimmond, C. S. B., Fortuniak, K., Klysik, K. and Oke, T. R. 2006. Temporal variations in heat fluxes over a central European city centre. *Theor. Appl. Climatol*. **84**, 103–115.

Oke, T. R. 2006. Initial guidance to obtain representative meteorological observations at urban sites: Instrument and Observing Methods (IOM). *WMO* **81**, 1–51.

Oke, T. R. 1988. The Urban Energy-Balance. *Prog. Phys. Geogr*. **12**, 471–508.

Pigeon, G., Lemonsu, A., Grimmond, C. S. B., Durand, P., Thouron, O. and co-authors. 2007. Divergence of turbulent fluxes in the surface layer: case of a coastal city. *Bound. -Layer Meteorol*. **124**, 269–290

Rannik, Ü. and Vesala, T. 1999. Autoregressive filtering versus linear detrending in estimation of fluxes by the eddy covariance method. *Bound. -Layer Meteorol*. **91**, 259–280.

Rannik, Ü., Vesala, T. and Keskinen, R. 1997. On the damping of temperature fluctuations in a circular tube relevant to the eddy covariance measurement technique. *J. Geophys. Res. Atmos*. **102**, 12789–12794.

Rannik, Ü., Keronen, P., Hari, P. and Vesala, T. 2004. Estimation of forest-atmosphere CO_2 exchange by eddy covariance and profile techniques. *Agric. For. Meteorol*. **126**, 141–155.

Raupach, M. R., Rayner, P. J., Barrett, D. J., DeFries, R. S., Heimann, M. and co-authors. 2005. Model-data synthesis in terrestrial carbon observation: methods, data requirements

and data uncertainty specifications. *Global Change Biol.* **11**, 378–397.

Richardson, A. D., Hollinger, D. Y., Burba, G. G., Davis, K. J., Flanagan, L. B. and co-authors. 2006. A multi-site analysis of random error in tower-based measurements of carbon and energy fluxes. *Agric. For. Meteorol.* **136**, 1–18.

Rotach, M. W. L., Vogt, R., Bernhofer, C., Batchvarova, E., Christen, A. and co-authors. 2005. BUBBLE – an urban boundary layer meteorology project. *Theor. Appl. Climatol.* **81**, 261.

Sailor, D. J. and Lu, L. 2004. A top-down methodology for developing diurnal and seasonal anthropogenic heating profiles for urban areas. *Atmos. Environ.* **38**, 2737–2748.

Sailor, D. J. 2011. A review of methods for estimating anthropogenic heat and moisture emissions in the urban environment. *Int. J. Climatol.* **31**, 189–199.

Steinecke, K. 1999. Urban climatological studies in the Reykjavik subarctic environment, Iceland. *Atmos. Environ.* **33**, 4157–4162.

Su, H. B., Schmid, H. P., Grimmond, C. S. B., Vogel, C. S. and Oliphant, A. J. 2004. Spectral characteristics and correction of long-term eddy-covariance measurements over two mixed hardwood forests in non-flat terrain. *Bound. -Layer Meteorol.* **110**, 213–253.

Vesala, T., Järvi, L., Launiainen, S., Sogachev, A., Rannik, Ü. and co-authors. 2008. Surface-atmosphere interactions over complex urban terrain in Helsinki, Finland. *Tellus Ser. B-Chem. Phys. Meteorol.* **60**, 188–199.

Vickers, D. and Mahrt, L. 1997. Quality control and flux sampling problems for tower and aircraft data. *J. Atmos. Ocean. Technol.* **14**, 512–526.

Vogt, R., Christen, A., Rotach, M. W., Roth, M. and Satyanarayana, A. N. V. 2006. Temporal dynamics of CO_2 fluxes and profiles over a central European city. *Theor. Appl. Climatol.* **84**, 117–126.

Walsh, C. J., Oke, T. R., Grimmond, C. S. B. and Salmond, J. A. 2004. Fluxes of atmospheric carbon dioxide over a suburban area of Vancouver. In: *Fifth Conference on Urban Environment*. pp. 1–5.

Webb, E. K., Pearman, G. I. and Leuning, R. 1980. Correction of flux measurements for density effects due to heat and water-vapor transfer. *Q. J. R. Meteorol. Soc.* **106**, 85–100.

Wienhold, F. G., Frahm, H. and Harris, G. W. 1994. Measurements of N_2O fluxes from fertilized grassland using a fast-response tunable diode-laser spectrometer. *J. Geophys. Res. Atmos.* **99**, 16557–16567.

Wilczak, J. M., Oncley, S. P. and Stage, S. A. 2001. Sonic anemometer tilt correction algorithms. *Bound. -Layer Meteorol.* **99**, 127–150.

Wilson, K., Goldstein, A., Falge, A., Aubinet, M., Baldocchi, D. and co-authors. 2002. Energy balance closure at FLUXNET sites. *Agric. For. Meteorol.* **113**, 223–243.

Wood, C. R., Lacser, A., Barlow, J. F., Padhra, A., Belcher, S. E. and co-authors. 2010. Turbulent flow at 190 m height above London during 2006–2008: a climatology and the applicability of similarity theory. *Bound. -Layer Meteorol.* **137**, 77–96.